

## Electron-spin-resonance studies of donors in wurtzite GaN

W. E. Carlos

*Naval Research Laboratory, Washington, D.C. 20375*

J. A. Freitas, Jr.

*Sachs Freeman Associates, Landover, Maryland 20785*

M. Asif Khan, D. T. Olson, and J. N. Kuznia

*APA Optics, Blaine, Minnesota 55434*

(Received 14 June 1993)

Electron-spin-resonance (ESR) measurements have been performed on a series of wurtzite GaN films grown on sapphire substrates by low-pressure metal-organic chemical-vapor deposition. The sample set included films grown with both AlN and GaN buffer layers. The ESR signal results from residual donors with  $g_{\parallel} = 1.9510$  and  $g_{\perp} = 1.9483$ . The  $g$  value and the effective mass can be explained using a five-band  $\mathbf{k}\cdot\mathbf{p}$  model. Nuclear hyperfine interactions are observed as a shift in the central resonance position, due to the Overhauser effect from which the density of the wave function at the Ga nucleus is derived. The ESR lines all have quite a sharp Lorentzian shape due to motional narrowing. At low temperatures ( $T < 20$  K) the linewidth narrows with increasing temperature, consistent with electrons hopping from donor site to donor site. At higher temperatures the line broadens due to electron-phonon interactions. The concentration of uncompensated donors is independent of film thickness for GaN buffered films but increases monotonically with thickness for AlN buffered films, probably due to a decrease in the concentration of compensating centers. Photoluminescence measurements indicate that only the thickest films are homogeneous along the growth direction.

### I. INTRODUCTION

Recent developments in heteroepitaxy have led to significant advances in single-crystal thin films of wurtzite-phase GaN grown on several different substrates, the most common being the basal plane of sapphire.<sup>1-5</sup> These films are generally  $n$  type with carrier concentrations between  $10^{16}$  and  $10^{19}$   $\text{cm}^{-3}$ , although insulating and  $p$ -type films have recently been reported.<sup>6,7</sup> The residual donor has not been positively identified, and  $N$  vacancies<sup>8,9</sup> and residual oxygen<sup>10</sup> have been proposed as possibilities. Many of the arguments used for these proposed donor identifications were based on the growth kinetics and chemical analysis of lower quality material which had been grown before higher purity source gases and advanced techniques became commonplace, and which typically had carrier concentrations in the range of  $10^{19}$   $\text{cm}^{-3}$ . It is not clear how applicable those arguments are to current materials with carrier concentrations of  $10^{16}$ – $10^{17}$   $\text{cm}^{-3}$ . In this work we focus on  $n$ -type (unintentionally doped) films with carrier densities  $< 2 \times 10^{17}$   $\text{cm}^{-3}$ . All samples were of the wurtzite polytype, which is the thermodynamically stable phase used in most previous studies. Electron-spin-resonance (ESR) measurements were performed on a series of different thicknesses of GaN films grown on sapphire substrates by low-pressure metal-organic chemical-vapor deposition. In particular, we examine a set of eight such films grown with either AlN or GaN buffer layers, and discuss the ESR signal resulting from residual donors.<sup>11,12</sup> Similar insulating films were also examined, but the resonance dis-

cussed in this work was only observed in the  $n$ -type samples and can, therefore, be associated with excess residual donors.

The association of the resonance with an impurity band of donors is briefly discussed in Sec. II. Detailed results of the experimental measurements are then divided into three sections which discuss the position of the resonance and its relationship to the band structure of GaN, the temperature dependence of the resonance position and the linewidths, and the dependence and homogeneity of the concentration of uncompensated donors on buffer layer and film thickness. Each of these results is discussed in detail in the separate sections, and then a brief summary of the results is given in Sec. VI.

### II. EXPERIMENT

The ESR measurements were performed in a Bruker 300ESP  $X$ -band (9.5 GHz) spectrometer equipped with a liquid-helium flow cryostat for temperature control. Typically the range of temperatures for the measurements was 2–50 K. There is a background signal due to transition metals in the sapphire substrates;<sup>13</sup> however, those lines saturate at low microwave powers (unlike the GaN donor line) and have a sharp angular dependence. Thus the donor line is readily separated by carefully aligning the samples and by saturating the substrate lines. The growth of the samples has been previously discussed<sup>3</sup> and these specific samples are the same ones used in the work of Ref. 11. Hall measurements of carrier concentration were performed on each sample at 77 and 300 K.

Results of those measurements are included in Table I, along with other sample characteristics. Low-temperature (6 K) photoluminescence measurements were performed on each sample using the 3.53 eV line of an argon-ion laser for excitation. Those results and their relationship to the question of film homogeneity will be briefly discussed in Sec. V, with a more complete presentation being the subject of a forthcoming paper.

In Fig. 1 we show a narrow portion of the ESR spectrum for a 3.1- $\mu\text{m}$  GaN film with a 25-nm-thick GaN buffer layer. The position of the resonance is  $B_0 = h\nu/g\beta - B_n$ , where  $\nu$  is the resonant frequency,  $\beta$  is the Bohr magneton,  $g$  is the Landé  $g$  value, and  $B_n$  is due to the effects of residual nuclear hyperfine interactions as discussed below. A sharp Lorentzian resonance line ( $\Delta B \approx 5G$  at 4.2 K) is observed at  $g_{\parallel} = 1.9510$  in all  $n$ -type samples and, as shown in the inset to Fig. 1, there is a slight anisotropy with the  $c$  direction as the principal axis and  $g_{\perp} = 1.9483$ . The orientation dependence of the  $g$  value is fit by  $(g_{\parallel}^2 \cos^2 \Theta + g_{\perp}^2 \sin^2 \Theta)^{1/2}$ , where  $\Theta$  is the angle between the  $c$  axis and the magnetic field. The degree of anisotropy ( $g_{\parallel} - g_{\perp}$ ) and the average  $g$  value are similar to those observed for donors in ZnO,<sup>14,15</sup> a semiconductor whose band structure is similar to that of GaN. Also included in Fig. 1 is a spectrum for the bare sapphire substrate which does not show this signal. This Lorentzian line is the only resonance which is clearly attributable to the GaN film and not to the sapphire substrate.

A number of factors support the association of the sharp resonance in Fig. 1 with donors in an impurity band. The average  $g$  value is near 2, as expected for donors or conduction electrons in a wide-band-gap semiconductor such as GaN, and the slight anisotropy is consistent with the hexagonal symmetry. The linewidth is much sharper than that for isolated centers in III-V semiconductors whose resonances are broadened by residual hyperfine interactions with the lattice nuclei.<sup>16</sup> In all of the samples used for this study the linewidth of this resonance narrows with increasing temperature up to  $T = T_{\text{min}}$ , due to exchange or motional averaging of the residual hyperfine broadening. A conduction-band ESR would not show this line narrowing; however, this is consistent with a resonance due to an impurity donor band for which the averaging interaction (and narrowing) increases with increasing temperature. Finally, the signal is not easily saturated by microwave power, consistent with

TABLE I. The properties of GaN thin films used in this study.

Sample	Buffer	Thickness ( $\mu\text{m}$ )	$n(77\text{ K})$ ( $\text{cm}^{-3}$ )	$n(300\text{ K})$ ( $\text{cm}^{-3}$ )	ESR density ( $\text{cm}^{-3}$ )
1	AlN	0.5	$7.1 \times 10^{16}$	$2.6 \times 10^{17}$	$2.4 \times 10^{16}$
2	AlN	3.3	$3.6 \times 10^{16}$	$1.2 \times 10^{17}$	$4.0 \times 10^{16}$
3	AlN	6.25	$3.7 \times 10^{16}$	$1.6 \times 10^{17}$	$8.2 \times 10^{16}$
4	AlN	10.6	$7.0 \times 10^{16}$	$2.4 \times 10^{17}$	$1.2 \times 10^{17}$
5	GaN	0.5	$3.4 \times 10^{16}$	$2.1 \times 10^{17}$	$6.0 \times 10^{16}$
6	GaN	3.1	$2.3 \times 10^{16}$	$1.1 \times 10^{17}$	$5.8 \times 10^{16}$
7	GaN	7.0	$2.4 \times 10^{16}$	$1.1 \times 10^{17}$	$4.4 \times 10^{16}$
8	GaN	9.3	$2.8 \times 10^{16}$	$1.3 \times 10^{17}$	$5.9 \times 10^{16}$

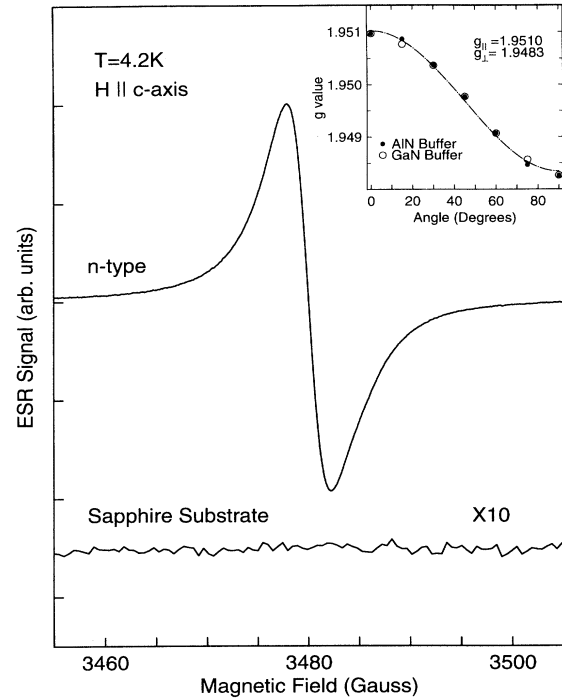


FIG. 1. The ESR signal due to excess donors in a GaN. The signal due to the substrate is included for comparison. The inset gives the angular dependence (with respect to the  $c$  axis) of the donor resonance.

a delocalized center rather than a localized one. To summarize the identification of the resonance: the  $g$  value indicates a resonance due to electrons in the conduction band or in a shallow donor level; the line shape and the temperature and microwave power dependencies of the linewidth are consistent with a donor band rather than isolated donors or electrons actually in the conduction band.

### III. THE CONDUCTION-BAND $g$ VALUE

The  $g$  value of the conduction band,  $g_c$ , and its effective mass  $m^*$  (in the following we discuss only average values) for a range of semiconductors can be explained using a five-band  $\mathbf{k} \cdot \mathbf{p}$  model<sup>17</sup> in which

$$3 \left[ 1 - \frac{g_c}{g_e} \right] = P^2 \left[ \frac{\Delta_0}{E_0^2} + \lambda^2 \frac{\Delta'_0}{(E'_0 - E_0)^2} \right], \quad (1)$$

$$\frac{m_0}{m^*} - 1 = P^2 \left[ \frac{1}{E_0} - \frac{\lambda^2}{(E'_0 - E_0)} \right]. \quad (2)$$

This takes into account the interaction of the  $\Gamma_1$  conduction band with the spin-orbit split  $\Gamma_6$  valence and conduction bands. The matrix elements coupling the  $\Gamma_1$  conduction band and these two bands are  $P^2$  and  $\lambda^2 P^2$ , respectively. The band separations and their spin-orbit splittings are defined schematically in Fig. 2. The free-electron  $g$  value and mass are  $g_e$  (2.0023) and  $m_0$ , respectively. For a wide-band-gap material such as GaN, the spin-orbit splittings are much smaller than the energy

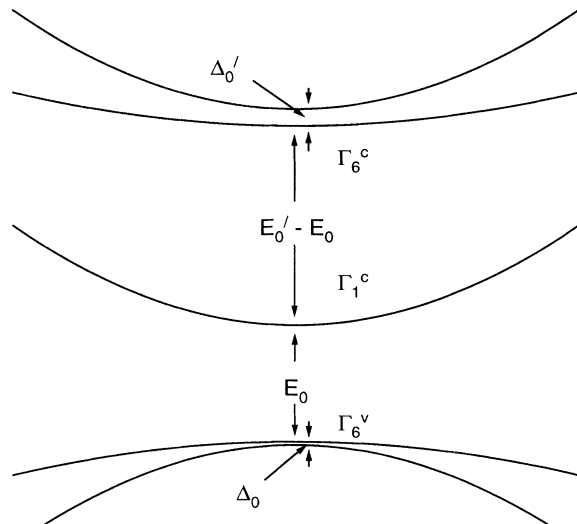


FIG. 2. The energy bands involved in the five-band  $\mathbf{k}\cdot\mathbf{p}$  calculation of the conduction-band  $g$  value and the electron effective mass. The energy spacings and band curvatures are not to scale.

gaps, and so they have been neglected in the energy denominators. The first term in the equation for  $g_c$  (due to the interaction with the valence band) dominates for many direct-gap semiconductors; however, this is not the case for GaN. The spin-orbit splitting of the valence band is due primarily to the anion (N) and is only 0.011 eV for GaN,<sup>18</sup> while that of the higher conduction band is due primarily to the cation (Ga) and might be expected to be comparable to that measured for other Ga compounds, e.g., 0.2 eV for GaAs.<sup>19</sup> Even though the second energy denominator  $(E'_0 - E_0)^2$  is larger than the first,  $E_0^2$ , the second term in the equation for  $g_c$  is then the larger of the two in the case of GaN. The two equations have a total of eight parameters; some are well established, some have experimental values with significant uncertainties, and others have no experimental values at all. The band gap,  $E_0$ ,<sup>20</sup> and, with present work,  $g_c$  clearly fit in the first group of well-established parameters; the uncertainty in either is less than 0.1%, which is insignificant compared to that of the other parameters. The conduction-band effective mass, which has been calculated from the infrared absorption due to free carriers,<sup>21</sup> is  $0.2m_0 \pm 10\%$ . The valence-band spin-orbit splitting is measured to be  $11 \pm 5$  meV<sup>18</sup> and  $E'_0$  is measured to be  $8.5 \pm 0.2$  eV (Ref. 22) from UV reflectivity measurements. This leaves three parameters which are unknown: the matrix elements coupling the conduction band with the valence band, with the higher conduction band, and with the spin-orbit splitting of the  $\Gamma_6$  conduction band. Using Eqs. (1) and (2) we can then relate two of these parameters as is shown in Fig. 3. Calculations on other III-V compounds which give accurate values for  $g_c$  and  $m^*$  yield between 15 and 30 eV for  $P^2$ ,<sup>17</sup> with the more ionic compounds having somewhat lower values; we can then set limits of  $10 < P^2 < 30$  eV. The ratio of

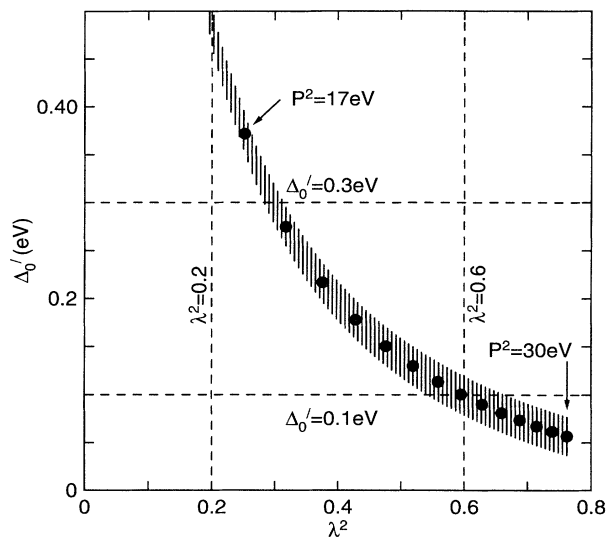


FIG. 3. The calculated spin-orbit interaction  $\Delta'_0$  as a function of  $\lambda^2$ . The dashed lines indicate the ranges  $0.3 > \Delta'_0 > 0.1$  eV and  $0.6 > \lambda^2 > 0.2$ , the points mark integer values of  $P^2$  along the curve, and the shading approximates uncertainties due to the parameters in Eqs. (1) and (2).

matrix elements  $\lambda^2$  is estimated to be on the order of 0.4,<sup>17,23</sup> although that is based on more covalent semiconductors such as GaAs, and so a prudent range may be  $0.2 < \lambda^2 < 0.6$ .<sup>24</sup> As mentioned above, the spin-orbit splitting of the  $\Gamma_6$  conduction band is primarily determined by the cation and therefore based on other Ga compounds,  $0.1 < \Delta'_0 < 0.3$  eV. These ranges are shown in Fig. 3 and their interactions further reduce these ranges of the parameter values to  $17 < P^2 < 23$  eV,  $0.46 < \lambda^2 < 0.60$ , and  $0.1 < \Delta'_0 < 0.3$  eV. The matrix element  $P^2$  can be crudely related to the effective masses of the valence bands,<sup>17</sup> and when experimental or theoretical values for those are available that will provide a further check on the parameters derived from the ESR measurements. As previously mentioned, we have only used an average value of  $g_c$  since the anisotropy of the effective mass has not been measured. When those results become available, we may be able to use the  $\mathbf{k}\cdot\mathbf{p}$  calculations to compare the anisotropies in the  $g$  and effective-mass tensors.

#### IV. LINE SHIFTS AND LINEWIDTHS

While the nuclear hyperfine interactions cannot be directly resolved, they manifest themselves as a shift in the central resonance position, due to the Overhauser effect. This effect has been observed in other III-V semiconductors.<sup>25-27</sup> The shift in the resonance is given by

$$B_n = \frac{A}{g_c \mu_B} \langle I_z \rangle, \quad (3)$$

where the hyperfine interaction is

$$A = \frac{4}{3} \mu_0 \mu_B \gamma_n \hbar |\Psi(0)|^2. \quad (4)$$

$\mu_B$  is the Bohr magneton,  $\gamma_n$  is the nuclear gyromagnetic ratio,  $\Psi(0)$  is the value of the wave function at lattice site, and the ensemble average of the nuclear polarization is given by

$$\langle I_z \rangle \approx \frac{\hbar \gamma_n I(I+1)B}{3kT} \quad (5)$$

for each lattice nucleus. Since  $^{69}\text{Ga}$  and  $^{71}\text{Ga}$  both have  $I = \frac{3}{2}$ , we use a simple weighted average of the  $\gamma_n$ 's for the two isotopes of Ga. The larger gyromagnetic ratios and spin of Ga indicate that the hyperfine interaction with the Ga nuclei should dominate and that to a first approximation the effects of the nitrogen nuclei may be neglected. We see from the above equations that the shift in the resonance position is proportional to  $B/T$ . In Fig. 4 we plot the observed resonance position as a function of inverse temperature, and from the intercept determine the resonance position in the absence of nuclear effects. This is  $B_0$ , which is used to determine the  $g$  value of the conduction band. From the slope and Eq. (4) we then calculate

$$|\Psi(\text{Ga})|^2 \approx 1.8 \times 10^{26} \text{ cm}^{-3}.$$

This is 2–3 times larger than has been found for In in InSb (Ref. 25) or InP,<sup>26</sup> and may be indicative of the electrons being more localized around lattice nuclei due both to the more ionic character of GaN and to the impurity banding. We emphasize that although the shift is primarily due to the interaction with the Ga nuclei, that is primarily due to the factor  $\gamma_n^2 I(I+1)$  being about 25 times larger for Ga than for N, rather than because the electrons are so much more localized around the Ga atoms. Similarly, in the case of InP the effect of the In is also much stronger (because  $I = \frac{9}{2}$  for In and  $I = \frac{1}{2}$  for P) but the electrons are only about twice as localized around

the In as around the P nuclei.<sup>27</sup> If a similar ratio were true for GaN, then the nuclear shift due to the N nuclei would only be about 2% of the total.

For all of the samples used in this work a minimum in the linewidth as a function of temperature is observed. In most films the temperature of the minimum is  $\sim 20$ – $30$  K, while in some cases it is as low as  $\sim 4$ – $6$  K. This general behavior is due to the competition between narrowing due to averaging of the residual hyperfine interactions at low temperatures ( $T < T_{\text{min}}$ ) and broadening due to electron-phonon interactions above  $T_{\text{min}}$ . In Figs. 5 and 6 we plot the linewidths of the donor ESR line for several representative samples. The data are identical for the two figures. In Fig. 5 the linewidth is plotted against inverse temperature to emphasize the low-temperature behavior, while in Fig. 6 the linewidths are plotted versus temperature to emphasize the behavior for  $T > T_{\text{min}}$ .

A decrease in linewidth with increasing temperature has been observed for donors in other semiconductors, e.g., P in Si,<sup>28,29</sup> As in Ge,<sup>30</sup> O vacancies in ZnO,<sup>14</sup> and residual donors in InSb.<sup>30</sup> These effects are attributed to an averaging of nuclear hyperfine interactions either through exchange interactions or through motion of the electrons from donor site to donor site in an impurity band. An increase in the exchange narrowing of the donor resonance with increasing temperature is attributed either to an increase in the conduction electron concentration and an increase in the interaction of the donor electrons with those electrons, or to an increase in the interaction between donor electrons as those become delocalized. Either is observed in a temperature regime where donors are becoming activated. In the present work, the narrowing is observed in the lowest-temperature regime ( $T < 20$  K in all cases) where the concentration of conduction electrons is constant but the donor electrons are already interacting. Therefore, we

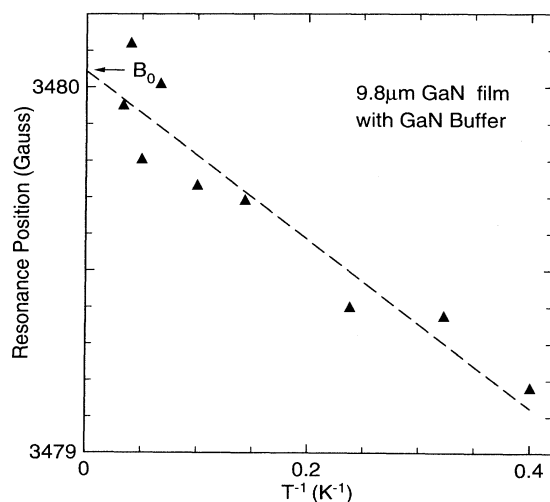


FIG. 4. The position of the donor resonance as a function of inverse temperature. The intercept is  $B_0$ , the position of the resonance without nuclear effects, which is used to determine the  $g$  value, while the slope is used to measure the nuclear hyperfine effects. The results shown are for sample 8.

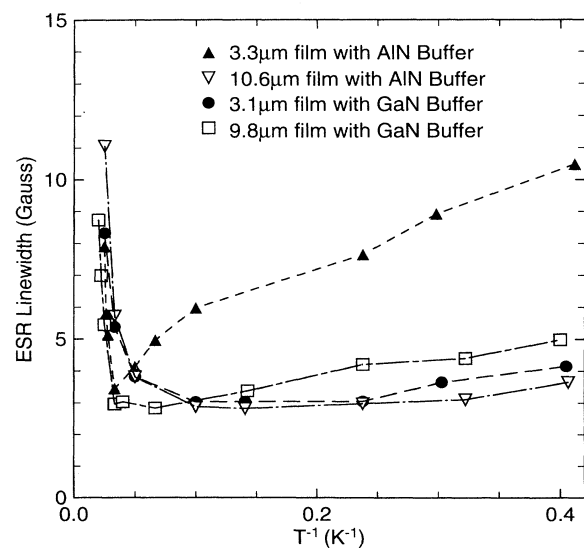


FIG. 5. The linewidths of several samples (2, 4, 6, and 8) as a function of reciprocal temperature. The dashed lines merely connect the points.

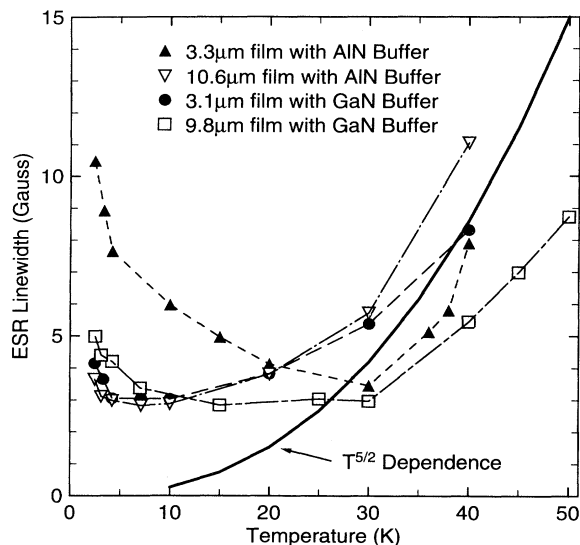


FIG. 6. The linewidths of the same samples, shown in Fig. 5, as a function of temperature. The bold line is a  $T^{5/2}$  fit to the combined data, while the dashed lines merely connect the points.

believe that the narrowing of the ESR line is due to motional effects rather than exchange interactions. The motion involved is similar to that involved in impurity band conduction,<sup>31</sup> and one might expect a small activation energy similar to that observed for such conductivity, e.g.,  $\sim 0.1$ – $1$  meV. From the data in Fig. 5 we can estimate activation energies of  $\sim 0.2$  eV, consistent with the idea of an electron hopping from donor site to donor site. Of course, one must be cautious in deriving too much from such a model, given that the linewidth changes over a relatively small temperature range,  $\sim 2$ – $20$  K, and we are not able to confidently rule out non-Arrhenius behavior or to determine if the linewidth has more than one component.

At higher temperatures the linewidth increases with increasing temperature due to the interaction of electrons with acoustic phonons. In semiconductors and metals the transverse relaxation time (the inverse of the linewidth) of delocalized electrons is approximately equal to the spin-lattice relaxation time  $T_1$ ,<sup>32</sup> which is related to the temperature and electron-phonon interaction by

$$\frac{1}{T_1} \propto \frac{T}{\mu_L}. \quad (6)$$

Here  $\mu_L$  is the lattice mobility, i.e., the electron mobility due to the electron-phonon interaction. At these low temperatures we limit  $\mu_L$  to the interactions with acoustic phonons. The lattice mobility is proportional to  $T^{-3/2}$  and so we expect the linewidth to vary as  $T^{5/2}$ . Furthermore, since  $\mu_L$  is an intrinsic property of the material there should not be appreciable sample-to-sample variation in the magnitude of the linewidths for  $T > T_{\min}$ . Both of these expectations are borne out in Fig. 6, where we see that the linewidths of different samples all follow

approximately the same power law, and for a given temperature show little variation in magnitude.

## V. DONOR CONCENTRATIONS AND DISTRIBUTIONS

Finally, we consider the intensity of the ESR line (measured at  $T=4.2$  K) and its variation with thickness and buffer layer. The ESR measurement determines the concentration of unionized uncompensated donors, while the Hall-Vander Pauw measurements determine the number of ionized uncompensated donors. In principle both the 300 K Hall and the low-temperature ESR measure  $N_D - N_A$ , the former measuring the number of conduction electrons in close to full ionization and the latter the number of neutral donors at close to complete freeze out. In Table I we see that the two measurements do scale reasonably well. There are, however, differences between the absolute values of the carrier density and the ESR density due to systematic errors in both measurements, and what is of more concern here are the relative variations rather than the factor  $\sim 2$ – $3$  between the ESR and Hall measurements. We note that both measurements give much less variation in the results for the samples with GaN buffer layers than for samples with AlN buffer layers. The concentrations for the former are also generally somewhat lower, which is in qualitative agreement with the results of Nakamura, Mukai, and Senoh,<sup>2</sup> who found superior films with GaN buffers.

For the AlN buffered films we see a monotonic increase in the uncompensated donor density with film thickness, whereas the films with GaN buffer layers have an almost constant density. This is illustrated in Fig. 7, in which we plot our ESR measurements of the concentration of excess donors as a function of film thickness. As discussed above, the densities scale reasonably well with the carrier concentrations measured at 300 K. We speculate that the increase in the *average* spin density with thickness for the films with AlN buffer layers has more to do with a decrease in the average density of compensating acceptors than with an actual increase in the density of donors. The origins of the acceptors may be the lattice and thermal expansion mismatch between the AlN buffer and the GaN film ( $\sim 2.5\%$  and  $\sim 33\%$ , respectively<sup>1</sup>). All of the films used in this work are much thicker than the critical thickness for GaN on AlN, and so dislocations near the film-buffer interface for the AlN buffered films could be a source of deep acceptors in those materials.

This suggests that inhomogeneities along the films' growth direction may be responsible for the thickness dependence of the ESR intensity. To further investigate this we have performed low-temperature photoluminescence with excitation (at 3.53 eV) at both the growth surface and the GaN-sapphire interface. The luminescence is primarily due to the GaN within a penetration depth ( $\sim 1$   $\mu\text{m}$ ) of the interface. A complete discussion of the luminescence results will be the subject of a separate paper. For excitation at the growth surface, the intensities of both near-band-edge luminescence and the deep yellow band centered at about 2.2 eV varied by  $\sim 3$  from sample to sample with no obvious trend. However, for excitation at the GaN-sapphire interface, both bands of the

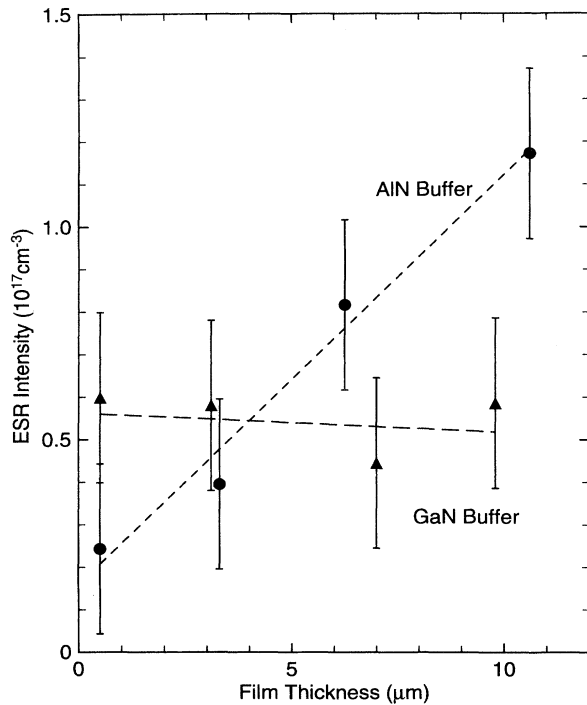


FIG. 7. The ESR intensity for samples with GaN and AlN buffer layers as a function of film thickness. The lines are included as an aid to the eye.

$\sim 3\text{-}\mu\text{m}$  films showed 1–2 orders of magnitude less intensity while the  $\sim 10\text{-}\mu\text{m}$  films had essentially the same intensity for excitation at either interface. This clearly indicates that the thinner films are not homogeneous but that as they grow their homogeneity improves, presumably due to annealing at the growth temperature.

There appear to be two luminescence quenching effects: compensation from acceptors (which may, in turn, be associated with dislocations) and nonradiative recombination centers. The former appears to be especially important in the AlN buffered samples and might offer an explanation of why the thinnest films actually have a lower ESR spin density than the corresponding GaN buffered film; i.e., the thinnest AlN buffered samples may be highly compensated. Nonradiative recombination centers also appear to play a significant role, especially in quenching the luminescence from the sapphire side of the GaN buffered samples. Clearly, more work is necessary to sort out the nature of structural defects in GaN films on sapphire, their relationship to the buffer layers, and their importance to recombination processes.

## VI. SUMMARY

We have presented a detailed discussion of our ESR measurements on a set of eight wurtzite GaN films on sapphire substrates. We observe a single resonance at  $g_{\parallel}=1.9510$  and  $g_{\perp}=1.9483$  due to a band of donors. The average  $g$  value can be used with other measured parameters and the standard five-band model to estimate ranges of values for the matrix elements coupling between the  $\Gamma_1$  conduction band and the  $\Gamma_6$  valence and conduction bands and the spin-orbit splitting of the  $\Gamma_6$  conduction band. In general, the parameters obtained are consistent with expectations from other III-V and II-VI semiconductors.

There is a slight temperature dependence to the resonance position which we attribute to residual hyperfine interaction with lattice nuclei (primarily Ga), as has been observed in other III-V semiconductors. We note that slight shifts in the resonance positions with temperature have been observed in other semiconductors whose lattice nuclei do not have magnetic moments, e.g., Si (Ref. 33) or ZnO.<sup>4</sup> In these cases the shifts are probably related to the transition from isolated donor electrons to delocalized electrons.

The ESR linewidths are determined by a competition between motional averaging of residual hyperfine interactions with lattice nuclei at low temperature and broadening due to electron-phonon interactions at higher temperatures. This qualitative model adequately explains the minimum in the linewidths as a function of temperature which we observe in all of our samples. The detailed variations in the linewidth data do not seem to correlate well with other properties of the films.

We observe that the spin density at low temperatures, which should equal  $N_D - N_A$ , increases with increasing film thickness for samples with AlN buffer layers but is roughly constant for samples with GaN buffer layers. We suggest that this may indicate that the interfacial region of the films with AlN buffer layers are more compensated than those with GaN buffer layers. Photoluminescence measurements show that the thinner films also show more inhomogeneity along the  $c$  axis than do the thicker ones. We further suggest that defects result in nonradiative recombination centers as well as compensating acceptors, and that both of these defects anneal out as the sample grows thicker.

## ACKNOWLEDGMENTS

The authors wish to thank R. Kaplan, T. A. Kennedy, and E. R. Glaser for helpful discussions. This work was partially supported by the Office of Naval Research.

<sup>1</sup>For detailed reviews of work in the group-III nitrides, see S. Strite and H. Morkoç, *J. Vac. Sci. Technol. B* **10**, 1237 (1992); R. F. Davis, *Proc. IEEE* **79**, 702 (1991).

<sup>2</sup>S. Nakamura, T. Mukai, and M. Senoh, *Jpn. J. Appl. Phys.* **28**, L2112 (1989); *J. Appl. Phys.* **71**, 5543 (1992).

<sup>3</sup>M. Asif Khan, J. N. Kuznia, J. M. Van Hove, D. T. Olson, S. Krishnankutty, and R. M. Kolbas, *Appl. Phys. Lett.* **58**, 526 (1991).

<sup>4</sup>H. Amano, N. Sawaki, I. Akasaki, and Y. Toyoda, *Appl. Phys. Lett.* **48**, 353 (1986).

- <sup>5</sup>R. C. Powell, G. A. Tomasch, Y.-W. Kim, J. A. Thornton, and J. E. Greene, in *Diamond, Silicon Carbide and Related Wide Bandgap Semiconductors*, edited by J. T. Glass, R. Messier, and N. Fujimori (Materials Research Society, Pittsburgh, 1990), p. 525.
- <sup>6</sup>M. Asif Khan, R. A. Skogman, J. M. Van Hove, D. T. Olson, and J. N. Kuznia, *Appl. Phys. Lett.* **60**, 1366 (1992).
- <sup>7</sup>H. Amano, M. Kito, and K. Hiramatsu, *Jpn. J. Appl. Phys.* **28**, L2112 (1989).
- <sup>8</sup>M. Ilegems and M. C. Montgomery, *J. Phys. Chem.* **34**, 885 (1973).
- <sup>9</sup>H. P. Maruska and J. J. Tietjen, *Appl. Phys. Lett.* **15**, 327 (1969).
- <sup>10</sup>W. Seifert, R. Franzheld, E. Butter, H. Sobotta, and V. Riede, *Cryst. Res. Technol.* **18**, 383 (1983).
- <sup>11</sup>M. Asif Khan, D. T. Olson, J. N. Kuznia, W. E. Carlos, and J. A. Freitas, Jr., *J. Appl. Phys.* **74**, 5901 (1993); W. E. Carlos, J. A. Freitas, Jr., and M. A. Khan, *Bull. Am. Phys. Soc.* **38**, 621 (1993).
- <sup>12</sup>ESR of donors in zinc-blende phase films has also been reported by M. Fanciulli, T. Lei, and T. D. Moustakas, *Bull. Am. Phys. Soc.* **38**, 621 (1993).
- <sup>13</sup>D. S. McClure, *J. Chem. Phys.* **36**, 2757 (1962).
- <sup>14</sup>J. Schneider and A. Räuber, *Z. Naturforsch. Teil A* **16**, 712 (1961); A. Hausmann, *Z. Phys.* **237**, 86 (1970).
- <sup>15</sup>D. Block, A. Hervé, and R. T. Cox, *Phys. Rev. B* **25**, 6049 (1982).
- <sup>16</sup>For reviews of ESR applied to III-V semiconductors, see V. K. Bashenov, *Phys. Status Solidi A* **19**, 9 (1972); N. D. Wilsey and T. A. Kennedy, in *Microscopic Identification of Electronic Defects in Semiconductors*, edited by N. M. Johnson, S. G. Bishop, and G. D. Watkins (Materials Research Society, Pittsburgh, 1985), p. 309.
- <sup>17</sup>For a review of this application of the  $\mathbf{k}\cdot\mathbf{p}$  model, see C. Hermann and C. Weisbuch, in *Optical Orientation*, edited by F. Meier and B. P. Zakharchenya (North-Holland, Amsterdam, 1984), p. 463.
- <sup>18</sup>R. Dingle, D. D. Sell, S. E. Stokowski, and M. Ilegems, *Phys. Rev. B* **4**, 1211 (1971).
- <sup>19</sup>D. E. Aspnes, C. G. Olson, and D. W. Lynch, *Phys. Rev. B* **12**, 2526 (1975).
- <sup>20</sup>B. Monemar, *Phys. Rev. B* **10**, 676 (1974).
- <sup>21</sup>A. S. Barker, Jr. and M. Ilegems, *Phys. Rev. B* **7**, 743 (1973).
- <sup>22</sup>S. Bloom, G. Harbeke, E. Meier, and I. B. Orthenburger, *Phys. Status Solidi B* **66**, 161 (1974).
- <sup>23</sup>D. J. Chadi, A. H. Clark, and R. D. Burnham, *Phys. Rev. B* **13**, 4466 (1976).
- <sup>24</sup>R. R. L. Zucca and Y. R. Shen, *Phys. Rev. B* **1**, 2668 (1970).
- <sup>25</sup>M. Gueron, *Phys. Rev.* **135**, A200 (1964).
- <sup>26</sup>B. Clerjaud, F. Gendron, H. Obloh, J. Schneider, and W. Wilkening, *Phys. Rev. B* **40**, 2042 (1989); B. Gotschy, G. Denninger, H. Obloh, W. Wilkening, and J. Schneider, *Solid State Commun.* **71**, 629 (1989).
- <sup>27</sup>M. Krapf, G. Denninger, H. Pascher, G. Weimann, and W. Schlapp, *Solid State Commun.* **74**, 1141 (1990).
- <sup>28</sup>Daniel J. Lépine, *Phys. Rev. B* **2**, 2429 (1970).
- <sup>29</sup>S. Maekawa and N. Kinoshita, *J. Phys. Soc. Jpn.* **20**, 1447 (1965).
- <sup>30</sup>E. M. Gershenson, N. M. Pevin, and M. S. Fogelson, *Phys. Status Solidi* **38**, 865 (1970).
- <sup>31</sup>N. F. Mott and W. D. Twose, *Adv. Phys.* **10**, 107 (1961).
- <sup>32</sup>Y. Yafet, in *Solid State Physics*, edited by H. Ehrenreich and D. Turnbull (Academic, New York, 1963), Vol. 14, p. 1; R. J. Elliot, *Phys. Rev.* **96**, 266 (1955).
- <sup>33</sup>G. Feher, *Phys. Rev.* **114**, 1219 (1959).